Design of a Heme-Binding Four-Helix Bundle

Christin T. Choma,[†] James D. Lear,[†] Mark J. Nelson,[‡] P. Leslie Dutton,[§] Dan E. Robertson,[§] and William F. DeGrado*[,†,§]

Contribution from the DuPont Merck Pharmaceutical Company, DuPont Experimental Station, P.O. Box 80328, Wilmington, Delaware 19880-0328, DuPont Central Research and Development Department, DuPont Experimental Station, Wilmington, Delaware 19880-0328, and Johnson Research Foundation, Department of Biochemistry and Biophysics, University of Pennsylvania, Philadelphia, Pennsylvania 19104

Received May 26, 1993. Revised Manuscript Received October 19, 1993®

Abstract: The design and characterization of two synthetic peptides that self-assemble into heme-binding proteins are described. The peptides are intended to fold into a four-helix bundle and bind a single heme parallel to the helices in the bundle core using two histidine side chains as ligands. Both proteins bind a single heme in the binding pocket. In one protein there are comparable amounts of low- and high-spin hemes, while in the other low-spin heme predominates. In both proteins, the EPR spectra of the low-spin heme indicate bis-imidazole ligation. The results illustrate that subtle differences in packing, binding pocket flexibility, and ligand orientation can significantly influence the characteristics of functionalized peptides.

The design of novel proteins which are intended to adopt predetermined three-dimensional structures is providing insights into the mechanisms, dynamics, and thermodynamics governing protein structure, stability, and function. A variety of designed proteins have been described,[1] including a family of four-helix bundles designed by an incremental process:[2] α_1, a single-helix peptide that self-assembles into an α-helical tetramer; α_2, a two-helix peptide that dimerizes to form a four-helix bundle; and α_4, a single-chain polypeptide that folds into a four-helix bundle. These bundles are compact, possess a high degree of secondary structure, and are thermodynamically very stable. However, in common with most proteins designed to date, their folding is driven largely by nonspecific hydrophobic interactions; geometrical complementarity in the packing of internal side chains and specific hydrogen bonded interactions are lacking. Consequently, most designed proteins lack a fixed tertiary structure.[3] To induce more native-like characteristics, and as a prelude to the introduction of functionality and catalytic activity into the bundle, two Zn^{2+} binding sites have recently been incorporated near the surface of the α_2 and α_4 proteins.[4] Here we describe the design and characterization of two derivatives of α_2, each containing a binding site for heme (iron protoporphyrin IX) in the *interior* of the four-helix bundle. Such proteins could be developed into either a synthetic electron-transfer system or catalytic systems.

Examples of naturally occurring four-helix bundle cytochromes include the monomer of cytochrome *c'* and cytochrome *b*-562.[5] Both consist of four α-helices in a left twisted antiparallel bundle with a single heme enclosed in the bundle interior. In cytochromes, axial iron ligands are commonly a histidine/methionine pair (as in cytochrome *b*-562) or bis-histidine (as in cytochrome b_5).[6] Both ligation schemes normally produce 6-coordinate, low-spin iron. For the initial design of a synthetic four-helix cytochrome, we focused on bis-histidine coordination because the 2-fold symmetry of the structure simplified modeling and synthesis and allowed the complete protein to be generated by simple dimerization of two-helix monomers.

Experimental Section

Materials. Fmoc[7]-protected amino acids and PAL resin were purchased from Millipore. Hemes (iron protoporphyrin IX and zinc protoporphyrin IX) were obtained from Porphyrin Products. All chemicals were of the highest available grade and were used without further purification.

Peptide Synthesis. Using Fmoc-protected amino acids, peptides were synthesized by solid-phase peptide synthesis on PAL resin[8] using a Milligen Model 9050 peptide synthesizer. Fmoc L-amino acids (Fmoc-L-Arg-(PMC)-OH) and Fmoc L-amino acid pentafluorophenyl (OPfp) esters (Fmoc-L-Ala-OPfp, Fmoc-L-Cys(Trt)-OPfp, Fmoc-L-Glu(OtBu)-OPfp, Fmoc-L-Gly-OPfp, Fmoc-L-His(Boc)-OPfp, Fmoc-L-Leu-OPfp, Fmoc-L-Lys(Boc)-OPfp, Fmoc-L-Pro-OPfp, and Fmoc-L-Val-OPfp) were recirculated through the resin for 45 min; arginine, cysteine, histidine, and proline residues were double-coupled. To stabilize helix formation,[2] end charges were neutralized by acetylating the N-terminus and amidating the C-terminus of the peptide. Peptides were cleaved from the resin by stirring the dried resin for 2 h at 20 °C with 9:0.5:0.3:0.2 TFA:thioanisole:

* Corresponding author.
† DuPont Merck Pharmaceutical Company.
‡ DuPont Central Research and Development Department.
§ University of Pennsylvania.
® Abstract published in *Advance ACS Abstracts*, December 15, 1993.

(1) (a) Moser, R. M.; Thomas, B.; Gutte, B. *FEBS Lett.* **1983**, *157*, 247–251. (b) Richardson, J. S.; Richardson, D. C. *Trends Biochem. Sci.* **1989**, 304–309. (c) Morii, H.; Ichimura, K.; Uedaira, H. *Proteins* **1991**, *11*, 1133–1141. (d) Goraj, K.; Renard, A.; Martial, J. A. *Protein Eng.* **1990**, *3*, 259–266. (e) Regan, L.; Clark, N. D. *Biochemistry* **1990**, *29*, 10878–10883. (f) Hahn, K. W.; Klis, W. A.; Stewart, J. M. *Science* **1990**, *248*, 1544–1547. (g) Kaumaya, P. T.; Berndt, K. D.; Heidorn, D. B.; Trewhella, J.; Kèzdy, J. F.; Goldberg, E. *Biochemistry* **1990**, *29*, 13–23. (h) Hecht, M. H.; Richardson, J. S.; Richardson, D. C.; Ogden, R. C. *Science* **1990**, *249*, 884–891. (i) Klauser, S.; Gantner, D.; Salgam, P.; Gutte, B. *Biochem. Biophys. Res. Commun.* **1991**, *179*, 1212–1219. (j) Ghadiri, R. M.; Soares, C.; Choi, C. *J. Am. Chem. Soc.* **1992**, *114*, 825–831. (k) Chin, T.-M.; Berndt, K. D.; Yang, N.-C. *J. Am. Chem. Soc.* **1992**, *114*, 2279–2280. (l) Mutter, M.; Vulleumies, S. *Angew. Chem., Int. Ed. Engl.* **1989**, *28*, 535–554.

(2) (a) Ho, S. W.; DeGrado, W. F. *J. Am. Chem. Soc.* **1987**, *109*, 6751–6758. (b) Regan, L.; DeGrado, W. F. *Science* **1988**, *241*, 976–978. (c) DeGrado, W. F.; Wasserman, Z. R.; Lear, J. D. *Science* **1989**, *243*, 622–628.

(3) Betz, S. F.; Raleigh, D. P.; DeGrado, W. F. *Curr. Opin. Struct. Biol.* **1993**, *3*, 601–610.

(4) (a) Handel, T.; DeGrado, W. F. *J. Am. Chem. Soc.* **1990**, *112*, 6710–6711. (b) Handel, T.; Williams, S. A.; DeGrado, W. F. *Science* **1993**, *261*, 879–885.

(5) (a) Weber, P. C.; Bartsch, R. G.; Cusanovich, M. A.; Hamlin, R. C.; Howard, A.; Jordan, S. R.; Kamen, M. D.; Meyer, T. E.; Weatherford, D. W.; Xuong, N. G.; Salemme, F. R. *Nature* **1980**, *286*, 302–304. (b) Xavier, A. V.; Czerwinski, E. W.; Bethge, P. H.; Mathews, F. S. *Nature* **1978**, *275*, 245–247.

(6) Moore, G. R.; Pettigrew, G. W. *Cytochromes c. Evolutionary, Structural and Physicochemical Aspects*; Springer Verlag: New York, 1990; pp 15, 318–329.

(7) Abbreviations: Fmoc, 9-fluorenylmethoxycarbonyl; PAL, 5-(4-(aminomethyl)-3,5-bis(methyloxy)phenoxy)valeric acid; PMC, 2,2,5,7,8-pentamethylchroman-6-sulfonyl; OPfp, pentafluorophenyl; TFA, trifluoroacetic acid; DTT, dithiothreitol; DMSO, dimethyl sulfoxide; HPLC, high performance liquid chromatography; Tris-HCl, tris(hydroxymethyl)aminomethane hydrochloride; CD, circular dichroism; UV, ultraviolet; FPLC, fast performance liquid chromatography; ANS, 8-anilino-1-naphthalenesulfonate; GuHCl, guanidine hydrochloride; MW, molecular weight; $\bar{v}$, partial specific volume; M_b, buoyant molecular weight; E_h, ambient potential.

(8) Albericio, F.; Barany, G. *Int. J. Pept. Protein Res.* **1987**, *30*, 206–216.

0002-7863/94/1516-0856$04.50/0

$\alpha 2$:
Ac C G E L E E L L K K L K E L L K G P R R
G E L E E L L K K L K E L L K G *CONH2*

VAVH25:
Ac C G E L E E L L K K A K E L L K G P R R
G E V E E H L K K V K E L L K G *CONH2*

H25:
Ac C G E L E E L L K K L K E L L K G P R R
G E L E E H L K K L K E L L K G *CONH2*

RETRO:
Ac C G K L L E K V K K L H E E V E G R R P
G K L L E K A K K L L E E L E G *CONH2*

Figure 1. Sequences of α_2, $VAVH_{25}$, H_{25}, and retro. Note that the (S–S) complexes used in all experiments are dimers of each peptide made by oxidizing the N-terminal cysteine.

ethanedithiol:anisole. After washing with TFA, concentrating the filtrate, and precipitating the peptide with ether, approximately 10 mg of crude, dried peptide was dissolved in 4 M guanidine monothiocyanate with 2% DTT and injected into a 2.5- × 25-cm Vydac C_{18} column. Peptides were eluted at a flow rate of 10 mL/min using a linear gradient of aqueous acetonitrile containing 0.1% TFA and were then lyophilized. The peptides were homogeneous and of the appropriate composition, as assessed by analytical HPLC, amino acid analysis, and fast atom bombardment mass spectrometry.

Covalently coupled homodimers were formed by oxidizing the N-terminal cysteine in 12% DMSO, 50 mM Tris-HCl buffer, pH 7.1, for 16 h at 20 °C.[9] The extent of oxidation was assessed by analytical HPLC. In the event of incomplete oxidation, the oxidized peptide was purified by preparative HPLC; otherwise, DMSO was removed by dialysis using 100-Da cutoff dialysis tubing (Spectrum Laboratory Products). All peptides were lyophilized and stored at 4 °C. Amino acid analysis and fast atom bombardment mass spectrometry confirmed the expected compositions of the covalently-linked peptide dimers.

Introduction of Heme. Concentrated solutions of heme (approximately 1 mg/mL) were freshly prepared either in DMSO or, for CD measurements, in 0.01 M KOH (although high pH accelerates heme dimerization, trace DMSO interferes with CD measurements in the far UV). Approximately 1.5 molar equiv of heme was slowly added over 5 min to the rapidly-stirring peptides (dissolved in 50 mM Tris-HCl buffer, 100 mM NaCl, pH 7.5). Peptide–heme samples were equilibrated for at least 1 h at 20 °C before unbound heme was removed. For the designed heme-binding peptides, this was accomplished by passage through a Pharmacia Superdex FPLC column (1.3 × 31 cm) at a flow rate of 0.25 mL/min. However, Superdex stripped bound heme from the control peptides (α_2(S–S) and H_{25}(S–S), Figure 1); therefore, unbound heme was separated from these peptides by chromatography through a Sephadex G-50 column (1.6 × 100 cm) at a flow rate of 1 mL/min.

Size Exclusion Chromatography. A Sephadex G-50 column (1.6 × 100 cm) equilibrated with 50 mM Tris-HCl buffer, 100 mM NaCl, pH 7.5, was calibrated with apomyoglobin, bovine pancreatic trypsin inhibitor, carbonic anhydrase, cytochrome *c*, and oxidized insulin B chain. Each of the disulfide-linked peptide dimers (1.0 mg) was chromatographed at a flow rate of 0.4 mL/min. The eluent was monitored by measuring the absorbance at 220 nm, and the apparent molecular weights of the peptides were determined by interpolation. Heme–peptide complexes were prepared by adding a 3-fold molar excess of heme (1 mg/mL in DMSO) to the rapidly-stirring peptide solutions. After 2 h at 20 °C, the peptide–heme complexes were chromatographed as above; the eluent was monitored at 220 and 400 nm.

Peptide:Heme Stoichiometry. To determine the stoichiometry of heme binding, peptide concentrations in the most concentrated fractions from the G-50 column eluents were determined by amino acid analysis. Analyses were performed on a Beckman system 6300 high-performance amino acid analyser with a post-column ninhydrin detection system. Heme concentrations in the same eluent fractions were determined by the pyridine–hemochrome method.[10] Pyridine (1.0 mL of a 40% solution in 0.2 M NaOH) and 6 μL of 0.1 M $K_3Fe(CN)_4$ were added to 1.0 mL of eluent. After 10 min, the absorbance at 540 nm was measured on a Hewlett Packard 8452A diode array spectrophotometer. Solid sodium dithionite (1.0 mg) was added, and after further mixing for 10 min, the absorbance of the sample at 556 nm was measured. The extinction coefficient for Fe–protoporphyrin IX (reduced minus oxidized spectra, $A_{556} - A_{540}$) is 23.98 mM cm^{-1}.[10] Amino acid analyses and heme concentrations were determined in quadruplicate. Norleucine was added as an internal standard to the amino acid analysis samples; the analyses had a standard deviation of less than 5%.

Sedimentation Equilibrium Ultracentrifugation. Equilibrium sedimentation was performed using a Beckman XLA analytical ultracentrifuge. Each cell, assembled from a six-channel centerpiece with fused silica windows, was loaded with three peptide samples (1–10 μM in 10 mM Tris-HCl, 10 mM NaCl, pH 7.5); peptides both with and without bound heme were analyzed. Corresponding buffer solutions were loaded in the reference compartments. Samples were centrifuged for 28 h at 20 °C and 30 000 rpm. The distribution of peptide within the cell was determined by measuring the absorbance of the sample every 0.02 cm along the radial length of the cell (0.7 cm) at 220 nm (peptide only samples) and 400 nm (for peptide–heme samples). Five scans were averaged, and equilibrium was assumed when successive radial scans were identical.

Data from each cell were analyzed using the program XLAEQ (Beckman Instruments) to determine the buoyant molecular weight, M_b, of each peptide or peptide–heme complex. $M_b = M_w(1 - \bar{v}\rho)$, where M_w is the "gram-atom-based" ("actual") molecular weight, $\bar{v}$ is the peptide partial specific volume, and ρ is the solvent density. The randomness of the residuals from the curve-fitting tested the suitability of single species analysis to any given data set. For each data set, M_b values were converted to M_w using the peptide partial specific volume calculated from the weight average of the partial specific volumes of the individual amino acids.[11] In addition, since the experimentally-determined molecular weights are constrained to be integral multiples of the sequence-calculated values, the values of the partial specific volumes were recalculated for the theoretical molecular weights assuming n elementary sequence units per sedimenting species, where $n = 1$ represents one disulfide-linked (S–S) peptide (see Table 2).

In one data set (H_{25}(S–S) without heme), single species analysis was inappropriate due to increasingly large positive differences between the observed and the calculated optical densities with increasing radial position in the cell. This data set was fit to theoretical monomer–dimer equilibrium curves using the Beckman Instruments program EQASSOC. A significant baseline correction was necessary to achieve reasonable fits. The molar extinction coefficient, ϵ, at the wavelength used to measure the peptide concentration profile (220 nm) was calculated from the A_{220} of an H_{25}-(S–S) solution of known concentration (determined by amino acid analysis).

Fluorescence. Fluorescence emission spectra of Zn–protoporphyrin IX bound to the peptides were measured at 25 °C on a Spex Fluorolog fluorometer. The porphyrin (0.1 mg/mL) was dissolved in DMSO and slowly titrated into the rapidly-stirring peptide solutions (2 μM in 50 mM Tris-HCl, 100 mM NaCl, pH 7.5) to an equimolar final concentration. The samples were excited at 428 nm, and emission spectra were measured at 1 nm/s between 500 and 700 nm.

In order to estimate the effective polarity of the heme-binding sites in the different peptides, the same concentration of Zn–protoporphyrin IX as used above was added to either buffer or various organic solvents: trifluoroethanol, methanol, ethanol, or octanol. The fluorescence emission intensities of these samples were then measured as above. To determine if the presence of imidazole could cause increased fluorescence emission of Zn–protoporphyrin IX, imidazole was added to the buffer sample at a concentration of 20 μM and the fluorescence emission spectrum was measured again.

UV–Visible Spectroscopy. Spectra (300–600 nm) were measured on a Hewlett Packard 8452A diode array spectrophotometer. Heme was reduced by adding approximately 0.1 mg of solid sodium dithionite directly to the samples.

Determination of Dissociation Constants for Peptide–Heme Complexes. Iron protoporphyrin IX in 1.5 mL of 50 mM Tris-HCl, 100 mM NaCl, pH 7.5, was titrated with peptide (in the same buffer) in increments of 0.1 equiv ($VAVH_{25}$(S–S): 25 μM heme, 100 μM peptide stock solution; retro(S–S): 2.5 μM heme, 40 μM peptide stock solution). After each addition of peptide, the rapidly-stirring samples were equilibrated for 20 min at 25 °C, then UV–visible spectra (300–600 nm) were measured. The increase in absorbance at 410 or 412 nm with increasing peptide

(9) Tam, J. P.; Wu, C. R.; Liu, W.; Zhang, J. W. *J. Am. Chem. Soc.* **1991**, *113*, 6657–6662.
(10) Berry, E. A.; Trumpower, B. L. *Anal. Biochem.* **1987**, *161*, 1–15.
(11) Cohn, E. J.; Edsall, J. T. *Proteins, Amino acids and Peptides as Ions and Dipolar Ions*; Reinhold Publishing Corp.: New York, 1943; pp 370–377.

concentration was corrected for dilution and fitted by a single site binding equation[12] using KaleidaGraph (Synergy Software).

Exogenous Ligand Binding. An excess of heme was titrated into the peptides (30 μM in 50 mM Tris-HCl, 100 mM NaCl, pH 7.5), and unbound heme was removed as described above. These samples (with heme in the Fe^{3+} oxidized state) were titrated with buffered solutions of sodium azide or potassium cyanide (1 mM), and the increase in the absorbance at 418 nm (the Soret band maximum for the heme–cyanide complex) or 420 nm (maximum for the heme–azide complex) was measured by UV–visible spectroscopy. Where binding was observed, the data was corrected for dilution and fitted as above using KaleidaGraph.

EPR. EPR spectra were obtained using a Bruker ER200D spectrometer equipped with an Oxford Instruments ESR900 cryostat and a Bruker ESP1600 computer. The following conditions were used: T, 20 K; microwave frequency, 9.430 GHz; microwave power, 2 mW; modulation amplitude, 2.0 mT; sweep time, 0.332 mT/s; resolution, 0.217 mT/point. Backgrounds were removed from the sample spectra by subtracting the spectrum of the buffer.

Redox Potentiometry. The electrochemical midpoints of the peptide–heme complexes were determined by redox potentiometry.[13] Adjustments in the ambient potential (E_h) of the sample (4 mL of approximately 10 μM peptide–heme complex in 50 mM Tris-HCl, 100 mM NaCl, pH 7.5) were made by addition of 1–3-μL quantities of approximately 1 mM sodium dithionite or potassium ferricyanide solutions. Potentials between 200 and −400 mV were measured using a platinum redox electrode with a calomel reference (Radiometer). Redox mediators were used to equilibrate between the electrodes, the solution, and the heme: 10 μM each of *N*-methyldibenzopyrazine methosulfate, *N*-ethyldibenzopyrazine ethosulfate, phenazine, and pyocyanine; 15 μM each of 2-hydroxy-1,4-naphthoquinone, anthroquinone-2-sulfonate; 20 μM each of 1,2-naphthoquinone, 1,4-naphthoquinone, 1,4-benzoquinone and 30 μM duroquinone and 40 μM 2,3,5,6-tetramethyl-*p*-phenylenediamine. Samples were deoxygenated, placed in a sealed cuvette maintained under a stream of Ar, and stirred throughout the titration. In order to measure the change in intensity of the α-band after each addition of dithionite or ferricyanide, samples were scanned beween 500 and 600 nm (the α/β band region) using a dual wavelength spectrophotometer designed and built by the Biomedical Instrumentation Group of the Johnson Research Foundation. After fully reducing the system with dithionite, the sample was reoxidized in an incremental manner with ferricyanide to test the reversibility of heme reduction.

Spectra were fit to Voight functions by iteration using PEAKFIT (Jandel Inc.). The intensity of the α-band maxima of reduced minus fully oxidized spectra were plotted versus E_h, and the data were analyzed for the best fit to multiple Nerst equations.[13]

Circular Dichroism. Spectra were recorded on an Aviv 62DS spectropolarimeter connected to an IBM PC. The instrument was calibrated with a solution of recrystallized D-10-camphorsulfonic acid. A circulating water bath was used to maintain the temperature of the sample cell at 25 °C. Urea and guanidine hydrochloride (GuHCl) denaturation curves were generated by mixing aliquots of peptide (with or without bound heme) in 10 mM Tris-HCl, 10 mM NaCl, pH 7.5, with appropriate volumes of the buffer and denaturant stock solution (10 M urea in 10 mM Tris-HCl, 10 mM NaCl, pH 7.5, or 8 M GuHCl) and measuring ellipticity at 222 nm. Concentrations of the stock peptide solutions were determined in quadruplicate by amino acid analysis. Data were fit by assuming a two-state solvent denaturation function[14] to determine $\Delta G^{(H_2O)}$, the free energy of unfolding the peptide or peptide–heme complex in the absence of denaturant.

Modeling. Molecular modeling was carried out using Insight II on a Silicon Graphics Personal Iris, and energy minimization was performed using Discover on a 480 Cray; both computer programs are from Biosym Technologies.

Results and Discussion

Peptide Design. Computer modeling was used to modify the original four-helix bundle to coordinate a single iron protoporphyrin IX molecule in the center of the bundle, parallel to the helices. The position of the histidine ligand in the monomer was dictated by several considerations. The imidazole rings of the histidine pair were to face each other edge-on across the span of the bundle interior, only low-energy rotomers of the rings were allowed, and the heme was to be located in the hydrophobic interior of the bundle with only the propionic side chains exposed to the solvent. In addition, incorporation of heme into the bundle could not cause major distortions of the peptide backbone or displacement of the helices.

In the models, the heme was oriented to permit favorable ionic interactions between the propionic acid groups and the arginine side chains of the Pro-Arg-Arg loops linking the helices. To ensure an unambiguous dimeric aggregation state with both loops oriented at one end of the bundle, a cysteine was introduced at the N-terminus of the peptide and oxidized to form a homodimeric, disulfide-linked protein. Since the N-terminal Gly and Glu of each helix do not participate fully in helix formation,[15] the Cys-Gly-Glu linker was sufficiently long to prevent straining and distortion of the bundle. Disulfide-linked peptides are denoted by the suffix (S–S) below.

The parent peptide α_2(S–S) (Figure 1) was used as a control throughout this study. The initial model of the heme-binding peptide started with an energy-minimized structure of the α_2 four-helix bundle. The loops were not included in the early stages of the modeling process in order to give the helices more freedom to move and accommodate the bulky heme group. Possible positions for the histidine ligands were explored by replacing pairs of leucines with allowed histidine rotomers. It was found that replacing leucine 25 with histidine would position the heme near the center of the bundle and permit the heme propionates to interact with the arginines in the loops.

Two different orientations of the imidazole ring were investigated. In the first, $\chi_1 = -81°$ and $\chi_2 = -138°$. This pointed the N^δ of each histidine directly into the center of the bundle. The distance between the N^δ atoms was approximately 5 Å, suitable for simultaneous interaction of the nitrogens with a heme iron.[16] A heme was then positioned so that the iron complexed with the N^δ atoms. The side chains of neighboring leucine residues were cut back wherever they overlapped with the van der Waals surface of the heme: positions 22 and 29 were changed to valines and position 10 to alanine ($VAVH_{25}$(S–S), Figure 1). In several incremental minimizations, the peptide–heme complex was unfrozen and the loops and disulfide bond were added to the model. This structure showed good packing between the heme and the designed binding pocket (Figure 2).

The van der Waals fit between the cofactor and its binding site in $VAVH_{25}$(S–S) is very good. However, heme ligation in natural cytochromes always occurs through the N^ϵ rather than the N^δ. This is presumably because of unfavorable interactions between the histidine C^β methylene group and the heme ring. In the $VAVH_{25}$(S–S) model, steric interactions of the histidine side chain with the heme and surrounding peptide prevented the necessary rotation of the imidazole ring that would point the N^ϵ atoms into the bundle interior. In an attempt to mimic a natural b-type cytochrome more closely, a second set of torsional angles for the histidines was introduced into the original four-helix bundle model. The histidine rotomer conformation ($\chi_1 = -77°$ and $\chi_2 = 80°$) found in myoglobin and hemoglobin (taken from crystal structures in the Brookhaven protein data bank) was inserted in position 25 of each α_2 dimer. With this orientation, the N^ϵ atoms of the imidazole rings point directly at the center of the bundle but are too close together to permit insertion of a heme. To increase the distance between the two histidines, the two helix/loop/helix monomers were pulled approximately 4 Å apart. This provided good van der Waals interaction between the heme and the leucine side chains, but there was very little interaction between the α_2 monomers, and many of the leucine side chains as well as the edges of the heme were fully solvent exposed. This peptide (H_{25}-

(12) Lear, J. D.; DeGrado, W. F. *J. Biol. Chem.* **1987**, *262*, 6500–6505.
(13) Dutton, P. L. *Methods Enzymol.* **1978**, *54*, 411–435.
(14) Santoro, M. M.; Bolen, D. W. *Biochemistry* **1988**, *27*, 8063–8067.
(15) Osterhout, J. J.; Handel, T.; Na, G.; Toumadje, A.; Lang, R. C.; Connolly, P. J.; Johnson, W. C.; Live, D.; DeGrado, W. F. *J. Am. Chem. Soc.* **1991**, *114*, 331–337.
(16) Chakrabarti, P. *Protein Eng.* **1990**, *4*, 57–63.

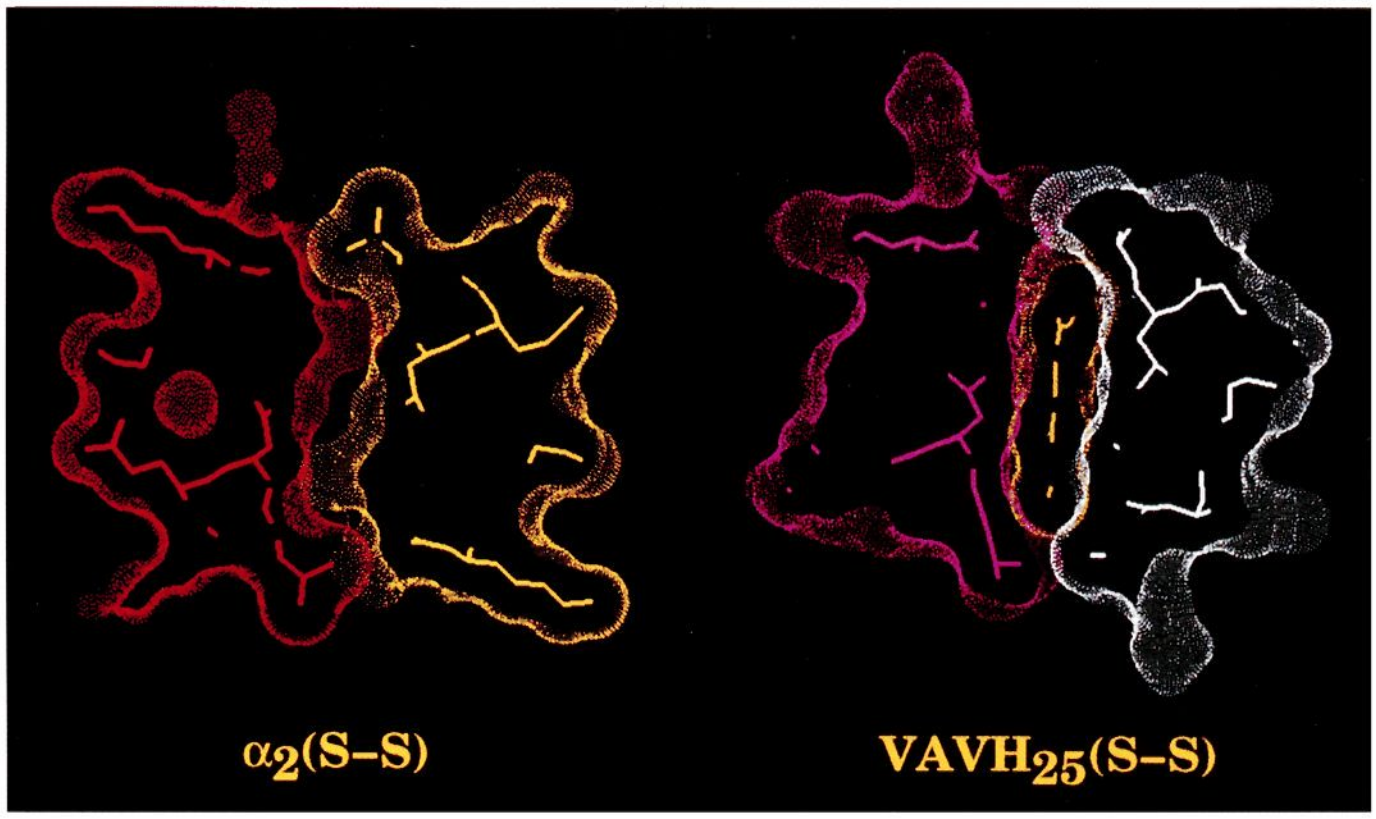

Figure 2. Energy-minimized models of (left) α_2(S–S), showing the shape complementarity of packing of the two halves of the bundle, and (right) $VAVH_{25}$(S–S), showing good van der Waals interactions between the bound heme and the binding pocket. The surface was created using the Connelly solvent-accessible surface algorithm as implemented by Insight II. This in effect rolls a 1.4-Å solvent ball on the surface of the protein. The solvent was rolled over each helix/loop/helix monomer of the bundle and on the surface of the heme.

(S–S), Figure 1) was deemed unlikely to bind heme, but it served as an important control to determine whether merely substituting two histidine residues into the hydrophobic core of the bundle would be sufficient to bind heme tightly and specifically.

In the course of this work, the reverse sequence of $VAVH_{25}$-(S–S) was synthesized and was found to bind heme. Reversing the sequence of the peptide would convert previously stabilizing interactions between charged side chains and the helix macrodipole into destabilizing interactions. This sequence (retro(S–S), Figure 1) was modeled from first principles. Two copies of the reverse sequence of $VAVH_{25}$ were built into a four-helix bundle. The helices were adjusted to position the apolar side chains in the interior of the bundle and to point the histidine imidazoles toward the centrally-positioned heme. Although the side chains in retro-(S–S) are less well packed than in $VAVH_{25}$(S–S) and the side chains project from the helices with significantly different geometries, the two models are overall similar (Figure 3). Interestingly, although we did not attempt an exhaustive search of helix/helix geometries, those geometries which were manually sampled could only ligate the heme iron through the N^{ϵ} atoms of both histidines.

Stoichiometry of Heme Binding. The four peptides (α_2(S–S), $VAVH_{25}$(S–S), H_{25}(S–S), and retro(S–S)) were synthesized and characterized. Physical and spectroscopic measurements (see below) showed that, in the absence of added heme, α_2(S–S), H_{25}(S–S), and $VAVH_{25}$(S–S) are fully folded and retro(S–S) is partially folded. Presumably all the peptides form four-helix structures. The stoichiometry of heme binding by the peptides was studied following size exclusion chromatography. After the addition of excess iron protoporphyrin IX to each peptide, the samples were chromatographed through a Sephadex G-50 column and the concentrations of peptide and heme in the peak fractions were determined. Heme was observed to bind to all the peptides, but the color of the peptide–heme complexes differed, suggesting different modes of binding: at approximately 10 μM peptide concentration, α_2(S–S) and H_{25}(S–S) were green, $VAVH_{25}$(S–S) was yellow–pink, and retro(S–S) was bright pink. The stoichiometry of heme binding was 1:1 for all the peptides, including the α_2(S–S) control (Table 1).

Hydrodynamic Studies. The effect of bound heme on the hydrodynamic radii of the peptides was also studied by size exclusion chromatography. Peptide samples containing a 3-fold excess of heme, and peptide samples without heme, were individually chromatographed through a calibrated Sephadex G-50 column. The elution volume of each sample was converted to the apparent molecular weight of the peptide (Figure 4). In the absence of heme, α_2(S–S) gives an anomalously large apparent molecular weight by size exclusion chromatography, consistent with previous observations[2] and reflective of the partial molten globule nature of the α_2 dimer.[4] In the presence of heme, the overall size of the bundle almost doubles, suggesting that heme binding disrupts the packing of the bundle or causes aggregation. It has been observed previously that other hydrophobic molecules such as ANS bind to the apolar, molten globule-like interior of α_2 and α_4 bundles.[4]

Unlike α_2(S–S), the apparent molecular weight of H_{25}(S–S) in the absence of heme is consistent with its known mass, suggesting that the need to accommodate the hydrophilic histidine side chains on the otherwise hydrophobic face of the second helix forces the bundle into a less dynamic and more well-defined structure. Like α_2(S–S), however, bound heme either disrupts packing of the H_{25}(S–S) bundle or induces higher oligomerization states.

The molecular weight of $VAVH_{25}$(S–S) as determined by size exclusion chromatography is consistent with its true mass and does not change upon incorporation of heme. This suggests that $VAVH_{25}$(S–S) sequesters heme into the binding pocket and so does not experience an increase in the hydrodynamic radius upon binding heme.

Retro(S–S) shows a significantly larger apparent molecular weight than either of the other peptides in the absence of heme, but addition of heme results in a compact and presumably structurally more defined bundle (Figure 4). As explained above, α_2(S–S), H_{25}(S–S), and $VAVH_{25}$(S–S) have designed charged side chain interactions that interact favorably with the helix dipole.[2] Reversal of the sequence should therefore result in destabilization of the helical structure.[17] The addition of heme apparently triggers the folding of retro(S–S) into a more compact structure, and the heme presumably serves as a template to stabilize the assembly.

Sedimentation Equilibrium Studies. In order to determine if the observed changes in apparent molecular size upon binding

(17) Marqusee, S.; Baldwin, R. L. *Proc. Natl. Acad. Sci. U.S.A.* **1987**, *84*, 8898–8902.

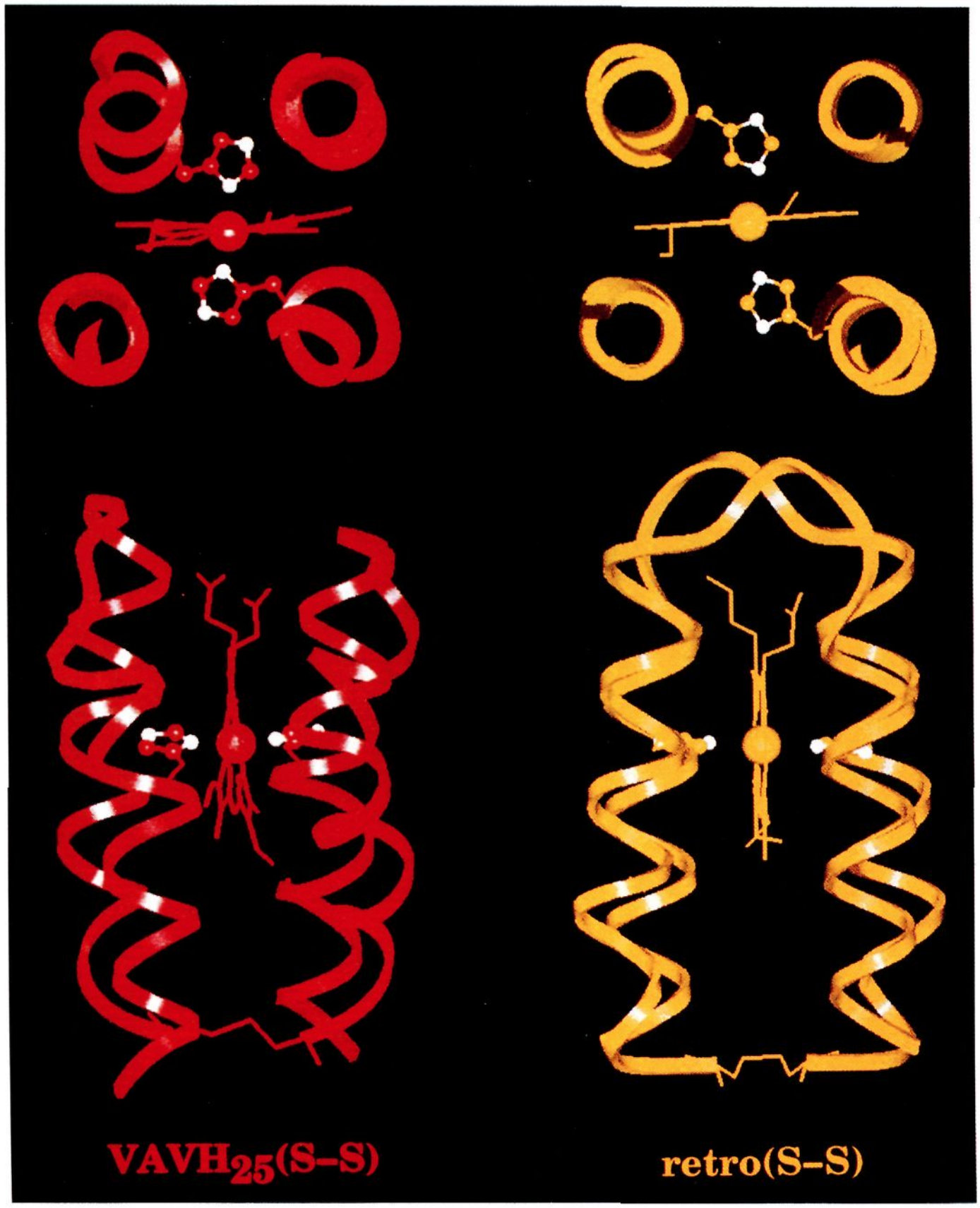

Figure 3. Energy-minimized models of (left) $VAVH_{25}$(S–S) and (right) retro(S–S), both with bound heme. Ribbons outline the trace of the peptide backbone. Only the histidine side chains are shown: nitrogens on the imidazoles are highlighted in white. Top: views looking down the core of each bundle at the heme-binding site. Bottom: lateral views of the proteins, with the loops positioned at the top and the disulfide positioned at the bottom of the bundles.

Table 1. Heme:Peptide Stoichiometry after Removal of Unbound Heme by Size Exclusion Chromatography[a]

α_2(S–S)	H_{25}(S–S)	$VAVH_{25}$(S–S)	retro(S–S)
0.98:1	1.02:1	1.0:1	0.97:1

[a] See the Experimental Section for details.

heme are due to changes in the self-association state, all the peptides, with and without bound heme, were subjected to equilibrium sedimentation. Table 2 gives the experimentally determined molecular weights of the proteins compared to those calculated from their amino acid sequences. In the absence of heme, all the proteins are essentially monomeric between 1 and 10 μM; in the presence of heme, $VAVH_{25}$(S–S) and retro(S–S) remain monomeric while both α_2(S–S) and H_{25}(S–S) form dimers. These results, together with the size exclusion data, indicate that the incorporation of heme by $VAVH_{25}$(S–S) does not have a significant effect on the hydrodynamic radius of the peptide, and that the heme is sequestered in the binding pocket. Further, the differences observed in apo-retro(S–S) and holo-retro(S–S) retention on the G-50 size exclusion column are reflective of a decrease in the overall size of the bundle, consistent with this peptide assuming a more compact and presumably more ordered structure upon the incorporation of heme.

The above calculations of molecular weight assume sequence-invariant partial specific volumes of peptide amino acid residues.[11] However, because we know the molecular weights of the peptides from their amino acid sequences and the aggregation states of all the peptides except apo-H_{25}(S–S), the partial specific volumes of the proteins can be recalculated with some confidence. The partial specific volumes of $VAVH_{25}$(S–S) and retro(S–S) (Table 2) are smaller than expected, indicating that the proteins are slightly denser than predicted from their amino acid sequences.

Characterization of the Heme Environment. Fluorescence. A major determinant of the quantum yield of fluorophores is the polarity and rigidity of the environment: the more apolar and rigid the environment, the greater the fluorescence intensity. To

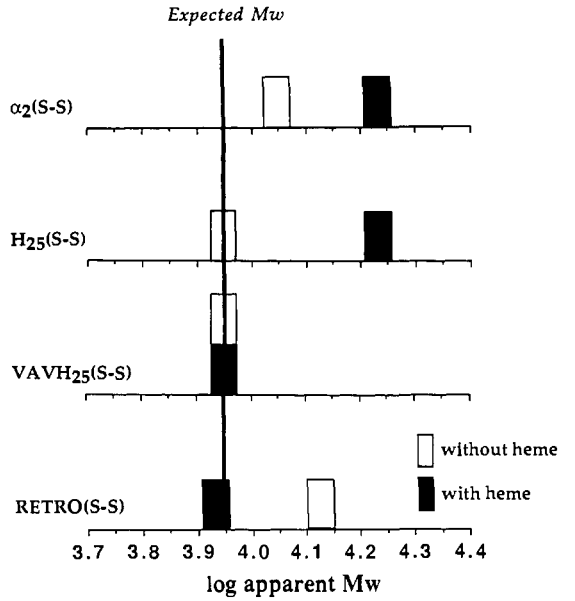

Figure 4. Apparent molecular weights of (from top) α_2(S–S), H_{25}(S–S), $VAVH_{25}$(S–S), and retro(S–S) in the absence (open symbol) and presence (shaded symbol) of heme. The expected molecular weight of all the peptides is approximately 8400. Procedural details are given in the Experimental Section.

Table 2. Theoretical and Measured Molecular Weights and Partial Specific Volumes of Peptides with and without Bound Heme

peptide	theor MW	measd MW[a]	calcd $\bar{v}$
α_2(S–S)	8 432	10 084	0.74
α_2(S–S) + heme	9 092	20 090	0.76
H_{25}(S–S)	8 474	~9 000[b]	na
H_{25}(S–S) + heme	9 134	21 702	0.74
$VAVH_{25}$(S–S)	8 342	7 588	0.80
$VAVH_{25}$(S–S) + heme	9 002	10 216	0.76
retro(S–S)	8 342	9 760	0.75
retro(S–S) + heme	9 002	10 547	0.75

[a] Molecular weights were calculated from analytical ultracentrifugation data using peptide partial specific volumes ($\bar{v}$) of 0.781 for α_2(S–S) and H_{25}(S–S) and 0.786 for $VAVH_{25}$(S–S) and retro(S–S). These values were calculated from the weight average of individual amino acid residue $\bar{v}$ values.[11] No account was taken of the effect of peptide end-caps or heme group inclusion. The centrifuge data showed no indication of concentration-dependent association (except for apo-H_{25}(S–S); *cf.* below). Since the unit peptide molecular weights are known, the partial specific volumes could be recalculated from the centrifuge data using the known peptide unit molecular weights. On the basis of the data in column 2, monomeric species were assumed for all peptides except the heme-containing α_2(S–S) and H_{25}(S–S) samples, which were assumed to be dimeric. With the exception of the apo-$VAVH_{25}$(S–S) value, the recalculated partial specific volumes (column 3) fell between the values calculated from the amino acid composition and the 0.724 average reported for 141 randomly selected natural proteins at 20 °C.[26] [b] This data set (apo-H_{25}(S–S)) showed a poor fit to a single species model. However, a monomer–dimer model gave a satisfactory fit with a calculated dimer dissociation constant of about 40 μM. Since the maximum peptide concentration in the cell was about 10 μM, the data indicate that the H_{25}(S–S) peptide is only partially dimerized under the conditions of measurement.

calibrate the effect of polarity on the emission intensity of Zn–protoporphyrin IX (a fluorescent compound), the porphyrin (2 μM) was added to aqueous buffer both with and without added imidazole (20 μM) and to organic solvents with different polarities (Table 3). The presence of a 10-fold excess of imidazole over porphyrin had no effect on the quantum yield of the porphyrin.

To estimate the effective polarity of the heme-binding sites in each peptide, Zn–protoporphyrin IX was added in a 1:1 stoichiometry to each peptide (2 μM). The intensity of the fluorescence emission spectra of Zn–protoporphyrin IX bound to

Table 3. Fluorescence Intensity

Zn–Protoporphyrin IX (2 μM)		
solvent	rel intens[a]	λ_{max} (nm)
buffer	1	587
trifluoroethanol	2.3	583
methanol	14	587
ethanol	23	587
octanol	52	588
1:1 Peptide:Zn–Protoporphyrin IX (2 μM)[b]		
peptide	rel intens[a]	λ_{max} (nm)
α_2(S–S)	1.1	590
H_{25}(S–S)	2.6	592
$VAVH_{25}$(S–S)	7.5	593
retro(S–S)	8.9	594

[a] Relative to fluorescence intensity of 2 μM Zn–protoporphyrin IX in 5 mM Tris-HCl, 100 mM NaCl, pH 7.5.

the two control peptides (α_2(S–S) and H_{25}(S–S), Table 3) indicates that the porphyrin remains essentially solvent exposed. In contrast, porphyrins bound to $VAVH_{25}$(S–S) and retro(S–S) show an increase in fluorescence quantum yield. The porphyrin in these proteins appears to experience an effective polarity that is intermediate between those of trifluoroethanol and methanol. This environment is somewhat more polar than expected from the models, which show the heme essentially sequestered from the solvent. These results may indicate that heme bound to $VAVH_{25}$(S–S) and retro(S–S) is less sheltered by the protein matrix than originally thought. Alternatively, these results could be a consequence of zinc requiring only a single histidine to satisfy its coordination requirements, leaving a polar pocket which can accommodate water molecules proximal to the heme.

UV–Visible Spectra. The UV–visible spectra of the peptide–heme complexes indicate that heme is bound differently in $VAVH_{25}$(S–S) and retro(S–S), which have a heme-binding site, than in the controls α_2(S–S) and H_{25}(S–S). Oxidized and reduced hemes in the green α_2(S–S) and H_{25}(S–S) complexes give a very broad Soret band (Figure 5A,B), typical of heme in free solution. This suggests that in these peptides the heme binds to the bundle with no change in its coordination sphere. Thus, in the absence of a binding pocket, heme cannot interact with the histidines of H_{25}(S–S).

In contrast, the Soret band of the yellow–pink $VAVH_{25}$(S–S) complex is much sharper (Figure 5C) and is shifted to longer wavelengths (maximum at 412 nm). The shape and position of the Soret band in $VAVH_{25}$(S–S) is similar to that observed in natural cytochromes with 6-coordinate heme,[18] but unlike these cytochromes, the α/β band region (500–600 nm) does not distinctly split when the heme is reduced. The Soret band of the pink retro(S–S) complex is even sharper and further red-shifted (414 nm) (Figure 5D), and in addition, there is pronounced splitting of the α/β region upon reduction with dithionite (Figure 6). These spectral features are diagnostic of low-spin, 6-coordinate iron.[19] Presumably, the heme in retro(S–S) is ligated by two histidines.

Heme–Peptide Dissociation Constants. As described above, α_2(S–S), H_{25}(S–S), $VAVH_{25}$(S–S), and retro(S–S) retained bound heme in a 1:1 stoichiometry following passage through a size exclusion column. This indicates that all the peptides bind iron protoporphyrin IX with reasonable affinity. On the basis of previous experience with related peptides, we estimate K_d is less than 10 μM (W.F.D., unpublished results). The large shift in the wavelength maximum of the Soret band upon ligation of free heme by histidine permitted more precise values of K_d to be measured for $VAVH_{25}$(S–S) and retro(S–S). Solutions of the

(18) Moore, G. R.; Pettigrew, G. W. *Cytochromes c. Biological Aspects*; Springer Verlag: New York, 1987; pp 11–15.
(19) Babcock, G. T.; Widger, W. R.; Cramer, W. A.; Oerlling, W. A.; Metz, J. G. *Biochemistry* **1985**, *24*, 3638–3645.

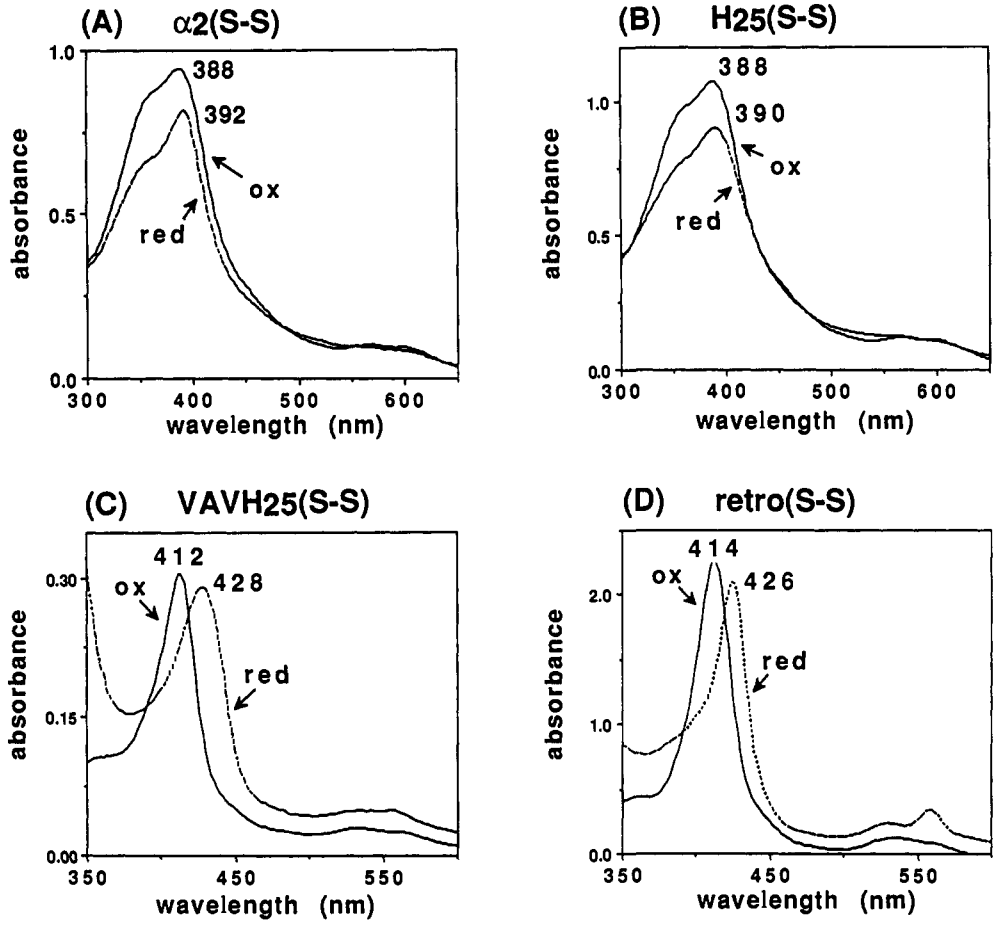

Figure 5. UV–visible spectra of Fe–protoporphyrin IX bound to (A) α_2(S–S), (B) H_{25}(S–S), (C) $VAVH_{25}$(S–S), and (D) retro(S–S): ox = oxidized (Fe^{3+}) heme; red = reduced (Fe^{2+}) heme. Heme was reduced by adding the minimum amount of solid sodium dithionite directly to the samples.

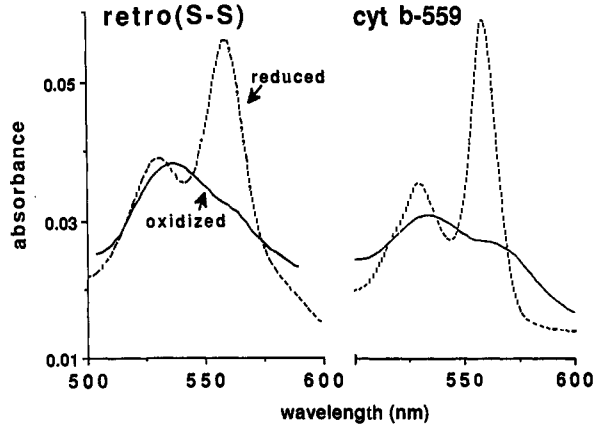

Figure 6. UV–visible spectra of the α/β region of oxidized (solid line) and reduced (dotted line) retro(S–S) complex (left) and cytochrome *b*-559[19] (right).

heme were titrated with peptide, and the increase in absorbance of the Soret band maximum at 410 or 412 nm was measured (Figure 7). $VAVH_{25}$(S–S) binds heme with an apparent dissociation constant of $(7 \pm 1) \times 10^{-7}$ M. It is difficult to determine the limits on the retro(S–S) K_d due to the lack of curvature in the data plot, but trial curve-fitting showed that K_d is considerably less than 1×10^{-7} M. The smaller K_d for retro-(S–S) is consistent with tighter coordination by the iron axial ligands.

Exogenous Ligands. Attempts to bind exogenous ligands further demonstrated differences in heme binding by the two peptides. Neither $VAVH_{25}$(S–S) nor retro(S–S) binds N_3^-, and retro(S–S) does not bind CN^-. However, $VAVH_{25}$(S–S) weakly binds CN^- with a $K_d \sim 4.5 \times 10^{-4}$ M. The best fit (lowest χ^2) to the data was obtained with a stoichiometry of 1 CN^- per $VAVH_{25}$(S–S). We conclude that the ferric iron in the retro-(S–S)–heme complex is inaccessible to exogenous ligands, consistent with strong internal 6-coordinate ligation, whereas in $VAVH_{25}$(S–S) exogenous ligands such as CN^- can access the heme and displace an axial ligand.

EPR. In order to confirm the coordination and spin state of the iron, EPR spectra of the ferric heme complexes of $VAVH_{25}$-(S–S) and retro(S–S) were obtained at 20 K, a temperature at which both low- and high-spin components are visible under nonsaturating conditions. The EPR spectrum of the ferric heme complex of retro(S–S) (Figure 8A) is dominated by a feature ($g_{z,y,x}$ = 2.97, 2.25, 1.51) arising from a low-spin ferric iron. The spectrum is diagnostic for a heme with two axial imidazole ligands where the planes of the imidazoles are roughly parallel to each other and to the Fe–N(pyrrole) bond of the heme.[20] In contrast, the EPR spectrum of $VAVH_{25}$(S–S) at 20 K shows roughly comparable contributions from low- and high-spin ($g \cong 6$) components (Figure 8B). Note that the low-spin feature is identical in the retro(S–S) and $VAVH_{25}$(S–S) heme complexes, confirming bis-histidine coordination of the heme in both cases. The presence of large amounts of high-spin heme in the $VAVH_{25}$-(S–S) complex and its virtual absence in retro(S–S) must reflect differences in coordination of the heme by the two peptides. It is possible that bis-histidine coordination of iron is somehow less stable in $VAVH_{25}$(S–S) than in retro(S–S), resulting in a significant population in which one imidazole has been displaced

(20) (a) Gadsby, P. M. A.; Thomson, A. J. *J. Am. Chem. Soc.* **1990**, *112*, 5003–5011. Certain cytochromes *c* with his/met ligation have EPR spectra very similar to those of bis-histidine hemes, but there is no possibility of methionine ligation in retro(S–S) or $VAVH_{25}$(S–S). (b) Teixeira, M.; Campos, A. P.; Aguiar, A. P.; Costa, H. S.; Santos, H.; Turner, D. L.; Xavier, A. V. *FEBS Lett.* **1993**, *317*, 233–236.

(21) Beetlestone, J.; George, P. *Biochemistry* **1964**, *3*, 707–714.

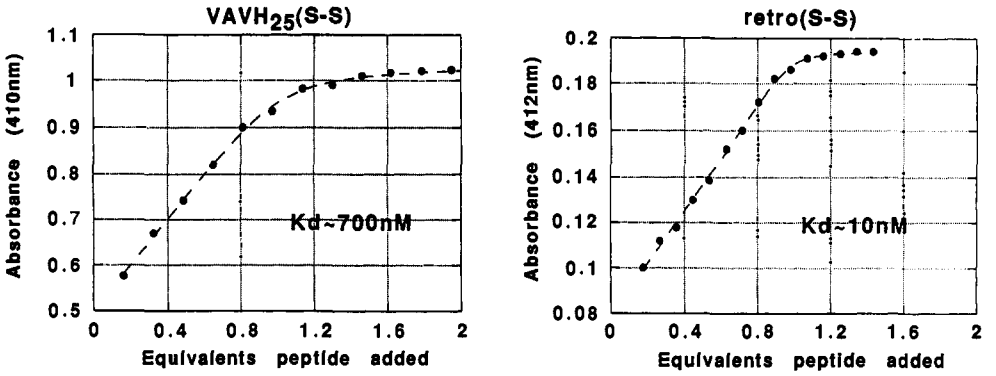

Figure 7. Determination of the peptide–heme K_d by measuring the increase in absorbance of Fe–protoporphyrin IX at 410 nm ($VAVH_{25}$(S–S)) and 412 nm (retro(S–S)) as the heme solution is titrated with peptide. Concentrations are as follows. $VAVH_{25}$(S–S): 25 μM heme, 100 μM peptide stock solution. Retro(S–S): 2.5 μM heme, 40 μM peptide stock solution. Procedural details are given in the Experimental Section.

by water or a chloride ion. We tend to discount this possibility because the affinity of the $VAVH_{25}$(S–S) complex for cyanide is very low (see above), much less than, for example, aquomet-myoglobin ($K_d = 7.1 \times 10^{-7}$ M),[21] suggesting the second axial ligand in the $VAVH_{25}$(S–S) complex is more tightly bound than one would expect a water to be.

A more plausible explanation is that the low-spin ↔ high-spin equilibrium observed in most heme-binding proteins (e.g., metmyoglobin)[22] is significantly more displaced in the direction of the high-spin form in the $VAVH_{25}$(S–S) complex compared to retro(S–S). This is consistent with the difference in heme ligation by the histidines in the two peptides predicted by molecular modeling (Figure 3). Retro(S–S) is predicted to coordinate the heme via the N^{ϵ} nitrogens of the imidazoles, consistent with all characterized protein–heme complexes.[6] In contrast, $VAVH_{25}$(S–S) is predicted to coordinate the heme using the N^{δ} nitrogens of the imidazoles. Steric interference between the C^{β} of the histidine side chains (α to the coordinating N^{δ}) and the porphyrin will lead to lengthening of the Fe–N^{δ} bonds and an increase in the high-spin character of the heme. This has precedent in the behavior of the synthetic complex bis(2-methylimidazole)-(octaethylporphyrinato)iron(III),[23] which is high-spin in the solid state as the result of steric interference between the 2-methyl of the imidazole (α to the coordinated nitrogen) and the porphyrin. In solution, this complex becomes low-spin because the imidazole is free to rotate and find a conformation that relieves the unfavorable steric interaction. In the $VAVH_{25}$(S–S) complex, the imidazole is presumably sufficiently constrained by interactions between the histidine side chain and the rest of the peptide to prevent a large proportion of the molecules from attaining the low-spin structure.

Redox Potentiometry. Redox titrations were conducted on all the peptide–heme complexes. The oxidized and reduced spectra of the control complexes (α_2(S–S) and H_{25}(S–S)) in the α/β region (500–600 nm) are too similar to allow measurement of redox potential by the method employed. The midpoint of the redox titration curve for the low-spin component of $VAVH_{25}$(S–S) (Figure 9A) is −170 mV, and for retro(S–S) (Figure 9B), −220 mV. A minor component with a midpoint of −90 mV present in the retro(S–S) titration curve is likely due to poor electrochemical equilibrium by the redox mediators;[24] this component is masked in the $VAVH_{25}$(S–S) titration curve by noise in the data. The midpoints measured for both peptide–heme complexes are in the range observed for natural cytochromes with bis-histidyl heme coordination with partially solvent-exposed hemes.[6]

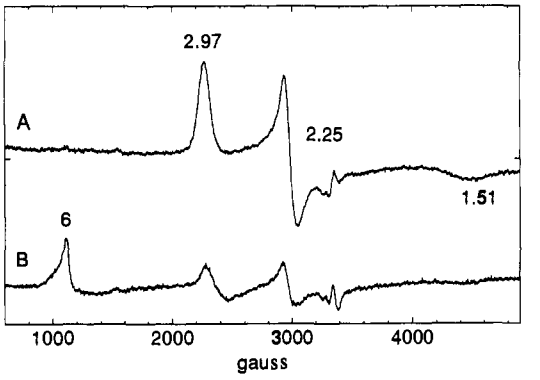

Figure 8. EPR spectra of (A) retro(S–S) and (B) $VAVH_{25}$(S–S) heme–peptide complexes. The small features between 3200 and 3400 G are artifacts resulting from background subtraction.

Stability of the Heme-Binding Peptides. Circular dichroism measurements showed that all the peptides except retro(S–S) have the same ellipticity at 222 nm (a measure of the helical content of a protein) in both the presence or absence of heme; the helical content of apo-retro(S–S) is about 20% less compared to the holoprotein. In order to estimate the energetic penalty for (i) introducing two histidines into the otherwise all-leucine interior of the bundle (H_{25}(S–S)), (ii) creating a cavity in the bundle interior ($VAVH_{25}$(S–S)), and (iii) reversing the direction of the helix dipole (retro(S–S)), the helicity of the peptides was measured at various concentrations of denaturant. The denaturation curves were fit by assuming a two-state solvent denaturation function[14] to determine $\Delta G^{(H_2O)}$, the free energy of unfolding the peptides in water.

The denaturation curves are shown in Figure 10. Since α_2-(S–S) does not unfold in urea,[2] denaturation curves for α_2(S–S) and H_{25}(S–S) were obtained in the stronger denaturant GuHCl, while the heme-binding peptides were denatured with urea. It is clear from Figure 10A that α_2(S–S) is extremely stable and does not denature appreciably at GuHCl concentrations less than 6 M; $\Delta G^{(H_2O)}$ is 13.5 ± 1.0 kcal/mol. In contrast, the stability and cooperativity of unfolding of H_{25}(S–S) is apparently compromised by the presence of two histidines on the otherwise hydrophobic face of the helix; the peptide is half unfolded in 4.5 M GuHCl, and $\Delta G^{(H_2O)}$ decreases by approximately 10 kcal/mol (to 2.8 ± 0.2 kcal/mol) compared to that of α_2(S–S).

Figure 10B shows that there is no change in the helical content of $VAVH_{25}$(S–S) upon binding heme and incorporating a heme in the binding pocket results in only a small increase in the stability of the peptide (from 2.1 ± 0.1 to 2.6 ± 0.2 kcal/mol). Interestingly, the stability of $VAVH_{25}$(S–S) in the absence of heme is similar to that of H_{25}(S–S), indicating that the energetic consequences of introducing the cavity-forming substitutions in the peptide sequence are rather small. In contrast, heme binding

(22) Kassner, R. J. *Biochim. Biophys. Acta* **1991**, *1058*, 8–12.
(23) Geiger, D. K.; Lee, Y. L.; Scheidt, W. R. *J. Am. Chem. Soc.* **1984**, *106*, 6339–6343.
(24) Dutton, P. L.; Wilson, D. F.; Lee, C. P. *Biochemistry* **1970**, *9*, 5077–5082.

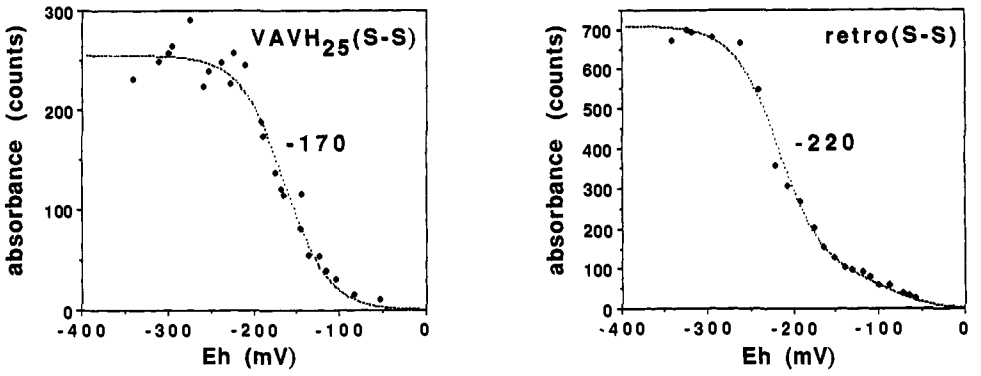

Figure 9. Redox titration curves of Fe–protoporphyrin IX bound to (left) $VAVH_{25}$(S–S) and (right) retro(S–S). The intensity of the α-band maxima (555 nm) of the reduced minus the fully oxidized spectra was plotted versus the ambient potential (E_h), and the data were analyzed for the best fit to multiple Nernst equations; good fits were obtained with $n = 1$. The E_h value at the midpoint in the titration is defined as the redox potential of the protein.

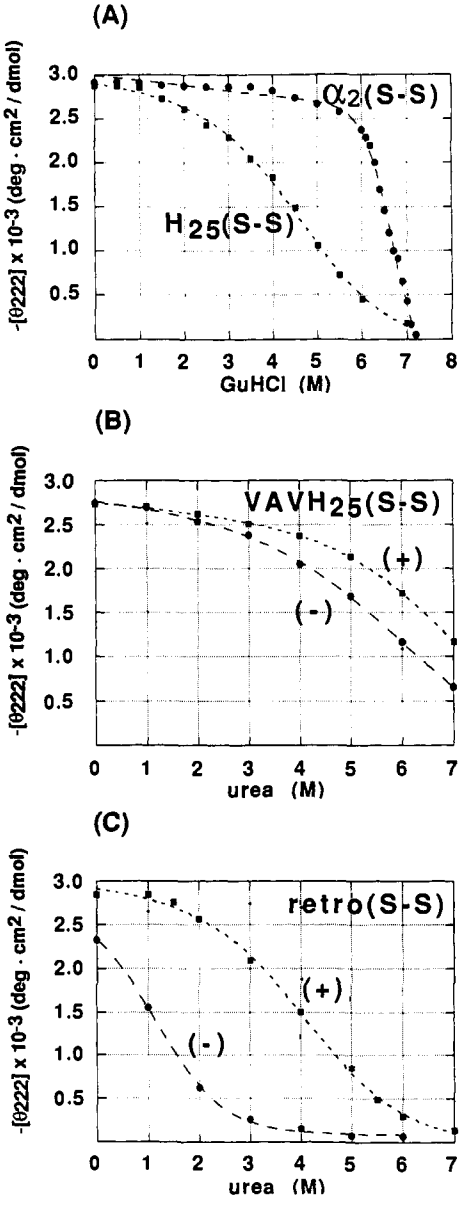

Figure 10. Denaturation curves of (A) α_2(S–S) and H_{25}(S–S) in GuHCl, (B) $VAVH_{25}$(S–S), with (+) and without (–) bound heme, in urea, and (C) retro(S–S), with (+) and without (–) bound heme, in urea.

has a larger impact on the structure of retro(S–S). The helical content of the peptide increases significantly (Figure 10C), as does its stability (from 1.1 ± 0.1 to 3.0 ± 0.2 kcal/mol).

The size exclusion and denaturation data show that retro(S–S) is only partially folded in the absence of heme and that heme presumably acts as a template around which the fully folded, more stable structure can form. The behavior of retro(S–S) is therefore similar to that observed for cytochrome c,[25a] cytochrome b_5,[25b,c] and cytochrome b_{562},[25d] where removal of the heme group disrupts the structure of the protein.

Conclusions

This paper describes the first examples of designed proteins that tightly and specifically bind a cofactor. The specificity of the design of $VAVH_{25}$(S–S) and retro(S–S) has been demonstrated by several controls. For example, although heme is bound stoichiometrically by both α_2(S–S) and H_{25}(S–S), the spectral properties of the bound heme indicate it is essentially solvent exposed. In addition, without the designed heme-binding cavity, α_2(S–S) and H_{25}(S–S) aggregate upon binding heme; the mere presence of two histidines within a semiflexible hydrophobic environment (H_{25}(S–S)) is insufficient to achieve specific binding. In contrast to the control peptides, $VAVH_{25}$(S–S) and retro(S–S) bind heme in a 1:1 stoichiometry and with high affinity in the heme-binding pocket. The spectral properties of retro(S–S) indicate that the heme experiences a well-defined environment and is bound predominantly in the low-spin state through two axial histidine ligands. The EPR spectrum of $VAVH_{25}$(S–S) shows that heme is in equilibrium with roughly equal amounts of high- and low-spin hemes; in the low-spin state at least, the two axial ligands are also histidines.

It is constructive to consider how the properties of $VAVH_{25}$(S–S) and retro(S–S) deviate from the expected properties of the design. Both peptides were designed to bind a single, buried, low-spin heme through two histidine ligands. Attempts to model heme-binding sites in the center of the α_2 bundle using low-energy rotomers of the histidine rings and the N^ϵ to ligate the iron led to unfavorable packing in the $VAVH_{25}$(S–S) complex. Therefore the model used the N^δ to ligate the iron although this gave rise to unfavorable van der Waals contacts between the heme ring and the C^β atom of the histidine. We cannot be certain that two histidines ligate the heme iron in the high-spin population of $VAVH_{25}$(S–S). However, the very weak affinity of the peptide–heme complex for CN^- suggests that the second histidine indeed interacts with the iron but that the Fe–N distances are too great to drive the iron into the low-spin state. In addition to potential constraints imposed on the spin state of the iron by steric interference between the histidines, the porphyrin, and the rest

(25) (a) Fisher, W. R.; Taniuchi, H.; Anfinsen, C. *J. Biol. Chem.* **1973**, *248*, 3188–3195. (b) Moore, C. D.; Lecomte, J. T. *Biochemistry* **1990**, *29*, 1984–1989. (c) Moore, C. D.; Al-Misky, O. N.; Lecomte, J. T. *Biochemistry* **1991**, *30*, 8357–8365. (d) Feng, Y.; Sligar, S. G. *Biochemistry* **1991**, *30*, 10150–10155.

(26) Attri, A. K.; Minton, A. P. *Anal. Biochem.* **1983**, *133*, 142–152.

of the peptide, $VAVH_{25}$(S–S) must contend with another limitation. Size exclusion chromatography and circular dichroism indicate that the peptide is fully folded in the absence of heme, and so perhaps it cannot freely explore all the conformations necessary to produce a 6-coordinate, low-spin heme.

$VAVH_{25}$(S–S) is a derivative of the original α_2 four-helix bundle, which was designed with specific stabilizing electrostatic interactions between charged residue side chains and the helix dipole. By reversing the sequence (as in retro(S–S)), previously stabilizing electrostatic interactions become destabilizing. Retro-(S–S) is therefore an inherently less stable protein than $VAVH_{25}$-(S–S). It is interesting to speculate that retro(S–S) can achieve full heme coordination by two histidine N^{ϵ} atoms precisely because it *is* less stable than $VAVH_{25}$(S–S) and is only partially folded in the absence of heme. It is therefore more flexible and is free to search a larger ensemble of conformers compatible with 6-coordinate low-spin heme. Our results suggest that a certain lack of preorganized structure in designed apoproteins is advantageous, and indeed some natural cytochromes are less structured in the apo form than in the holo form.[25]

The degree of solvation of the heme-binding site in $VAVH_{25}$-(S–S) and retro(S–S) differs somewhat from expectation. The models show the propionic groups of the heme exposed to the solvent in both peptides, and small sections of the vinyl groups in retro(S–S). However, the relatively negative redox midpoints of the peptides and the fairly low fluorescence intensity of Zn–protoporphyrin bound to both $VAVH_{25}$(S–S) and retro(S–S) suggest that the hemes are more solvent exposed than anticipated.

Given that the parent peptides α_2 and α_4 show some molten globule-like characteristics,[4] it is important to ask whether the heme complexes of $VAVH_{25}$(S–S) and retro(S–S) are uniquely folded. The presence of this state is usually assessed by NMR, the binding of apolar fluorophores such as ANS, and the measurement of temperature-induced unfolding to determined ΔC_p and the cooperativity of the unfolding process. Unfortunately, these peptide–heme complexes are insufficiently soluble at the concentrations required to permit NMR investigation of their structures, and the binding of ANS by the peptide–heme complexes could not be monitored because the heme would quench the ANS fluorescence. However, preliminary CD data from the thermal unfolding of $VAVH_{25}$(S–S) and retro(S–S) with and without bound heme (data not shown) are similar to that obtained from α_4.[4b] These preliminary studies also suggest that ΔC_p values for $VAVH_{25}$(S–S) and retro(S–S) are similar to that found for α_4, indicating that their interiors can be partially penetrated by water.

Despite the differences from the intended design, the present study demonstrates the feasibility of designing functional synthetic proteins. While rather subtle differences in binding pocket flexiblity and ligand orientation can have a large effect on the outcome of the design, it is now clear that proteins which bind cofactors and assume overall folds can be prepared. Furthermore, to the extent that the properties of the designed proteins fall short of expectation, it is generally possible to diagnose and, in future designs, remedy the potential problems associated with the initial designs.

The results of this paper indicate that it should be possible to prepare a variety of functional heme proteins. Our future studies will focus on the design of proteins with multiple redox-active centers capable of electron transfer.[27] In addition, proteins related to $VAVH_{25}$(S–S) could be used as model systems for studying oxygen binding and activation.

Acknowledgment. We thank Karin Akerfeldt for many helpful discussions, F. Ann Walker for critical reading of this manuscript, Jim Krywko and Zelda Wasserman for invaluable assistance with computer modeling and Rami S. Farid for helpful discussions. We thank Rich McKay for electrospray mass spectrometry of the peptides and Pat Webber for amino acid analyses. We also thank Emory Braswell of the Biotechnology Center, University of Connecticut (supported by a grant from the National Science Foundation), for preliminary sedimentation data and helpful advice.

(27) Robertson, D. E.; Farid, R. S.; Moser, C. E.; Pidikiti, R.; Lear, V. D.; DeGrado, W. F.; Dutton, P. L. Submitted for publication.